Chapter 2
3D Topology Optimization with Bricks

For thin panel topology optimization results to be practical from a manufacturing perspective, a number of key issues must be addressed. Firstly, the results should suggest a clear concept for the subsequent design process. In addition, a low number of optimization runs should provide good results. Also, visualization software must be available to efficiently recognize design features in the results. The aim of this work was to address these and other points in order to increase the usefulness of structural topology optimization for the design of thin-panel structures.

2.1 Spoiler Interior Structure Optimization

A density based topology optimization method was applied to a generic aircraft spoiler design problem with an emphasis on real-world design issues. Finite element analyses were performed using a 3D grid of identical 8-node brick elements and a checkerboard fill-in algorithm was used to exercise control over checkerboarding. Highly efficient computations were performed by storing the global stiffness matrix in implicit form and by using a Pre-conditioned Conjugate Gradient (PCG) solver. The mesh dimensions and volume constraint were varied in order to determine what parameters give topologies that are most suitable for subsequent conversion into real world, manufacturable designs.

A number of topology optimization runs were performed and a framework was created for comparing the results based on criteria relating to manufacturing feasibility. Procedures for converting the topology optimized structures into real-world design concepts were found by examining the set of results. One aim of this research was to provide better estimates for topology optimization control parameters for use in future studies on thin-panel structures.

2.1.1 Spoiler Design Problem

Figure 2.1 shows the design envelope of the generic spoiler design problem that was the subject of this research. This design envelope consists of a thin rectangular structure with three hinges, an actuator inputting a vertical load in the middle and a tapered trailing edge. Throughout this work a symmetry plane at the middle hinge was used for finite element modeling. The structure was subjected to a uniform 4 KPa pressure loading on the top surface.

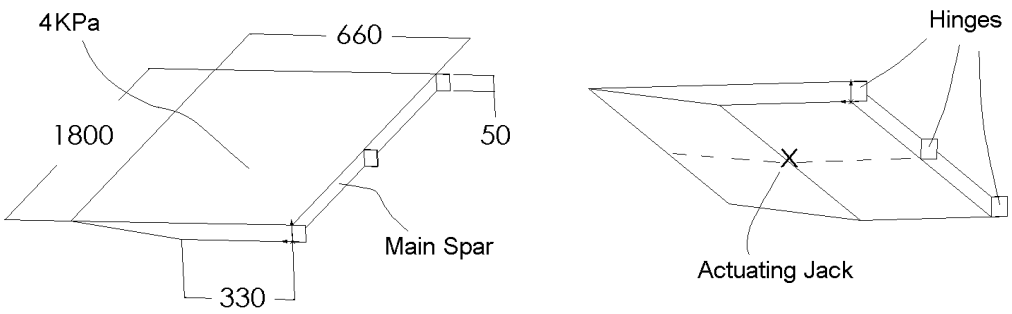

Figure 2.1, Spoiler design envelope; top view (left), bottom view (right).

In existing work (Ness *et al.*, 1998) a variety of problem formulations and a variety of structural optimization algorithms (both topology and sizing) were applied to determine structurally efficient design features of a generic spoiler manufactured from composite materials. It was concluded that the preferred structural configuration of the spoiler was based on span-wise stiffening of a torsion box. Further work presented in Chapter 4 of this thesis investigates minimizing the weight of a shell element model of the spoiler with a global buckling constraint and obtained data on the structural efficiency for a range of practical design concepts.

In all of the work mentioned above, finite elements extending from the top skin to the bottom skin of the spoiler were used. Hence, no distinction was made between the internal members attached to only one skin (e.g. conventional stiffeners) and those attached to both top and bottom skins (e.g. spars and ribs). Furthermore, the variation of the thickness of the top and bottom skins was restricted to be uniform or near uniform.

The objective of this research was to find the optimal 3D topology for the spoiler by minimizing the compliance of the structure. The optimization included both internal structure and external structure (i.e. skin) to determine if the optimal shape was truly available in the methodologies of previous work that used single elements through the thickness. Minimizing the compliance was desirable since it tended to minimize the tip deflection - an important factor in the aerodynamic and aero-elastic performance of a spoiler.

2.1.2 Efficient Computations

To minimize the time taken for large finite element analyses it is desirable to store the stiffness matrices in the most efficient format that is available. This allows larger problems to fit within the Random Access Memory (RAM) of the computer where the read/write access is relatively quick compared to accessing the hard drive. In work on by Hollister & Kikuchi (1994), a homogenization method to efficiently perform finite element calculations on grids of identical elements was presented. In both the Voxel Analysis method (Suzuki *et al.,* 1997) and the Fixed Grid Method (Garcia & Steven) uniform girds of equivalently sized finite elements were used to analyse solids. Although, the Voxel Analysis Method and the Fixed Grid Method used different boundary surface approximations, they both used Pre-conditioned Conjugate Gradient (PCG) solvers and stored the stiffness matrices in implicit data structures.

These implicit storage methods were achieved by recognizing the identical nature of the finite elements making up the models. In this work a similar finite element solution method was employed. However, the densities of each element were assigned as design variables and the relationship used by Yang & Chuang (1994) was assumed to exist between density and Young's modulus:

$$\frac{E_i}{E_0} = \rho_i{}^p , \qquad (2.1)$$

where E_i is the Young's modulus of element *i*, E_0 is the original Young's modulus, ρ_i is the density of the *i*'th element and *p* is a power term that penalizes intermediate densities (*p* was 2.0 in this work).

Due to the linearity of the element stiffness matrix terms with respect to modulus, the same $\rho_i{}^p$ can become the multiplier of an implicitly stored element stiffness matrix. Hence, all element stiffness matrices are merely linear multiples of the original element stiffness matrix. Thus, the global stiffness matrix was stored as,

$$\mathbf{K} = \sum_{i=1}^{N} \rho_i{}^p \mathbf{K}_e{}^* , \qquad (2.2)$$

where $\mathbf{K}$ is the global stiffness matrix, $\mathbf{K}_e{}^*$ is the element stiffness matrix (stored only once for the entire model),

A diagonally Pre-conditioned Conjugate Gradient (PCG) solver (Van Der Vorst & Dekker, 1988, 4.1) was used to take full advantage of the sparsity of the global stiffness matrix. As such, the evaluation of each matrix by vector operation in the PCG solver involved an extra multiplication to account for the density of the respective elements. However, the overall solution was more efficient since far larger problems could fit inside the RAM of the computer.

2.1.3 The Density Method

Minimization of the compliance was the optimization objective for this research. A good description of compliance minimization can be seen in Zhou & Rozvany's (1991) COC algorithm that was used for truss and plate optimization. The densities of each finite element were the design variables. Hence, the natural choice for the topology optimization algorithm was a density method. The software used in this study was a modified version of the software written for the Density Method for Topology Optimization (Fujii *et. al.*, 2000). In its original state, the Density Method software could only store the finite element model of structures that are perfect

rectangular prisms. The modifications made in this work were required to model structures with geometry like the spoiler.

According to (2.2), the density, and hence, Young's moduli of a large number of isotropic finite elements were adjusted to minimize the compliance of the structure under a volume constraint. The set of all element densities formed the design vector and the Optimality Criterion (OC) algorithm (Suzuki & Kikuchi, 1991) controlled the density of each finite element, ρ_i ($0 \le \rho_i \le 1$), according to,

$$\rho_i^{(k+1)} = \begin{cases} \max\left\{(1-\zeta)\rho_i^{(k)}, 0\right\} & \text{if} \quad s_i^{(k)} \le \max\left\{(1-\zeta)\rho_i^{(k)}, 0\right\} \\ s_i^{(k)} & \text{if} \quad \max\left\{(1-\zeta)\rho_i^{(k)}, 0\right\} \le s_i^{(k)} \le \min\left\{(1+\zeta)\rho_i^{(k)}, 1\right\} \\ \min\left\{(1+\zeta)\rho_i^{(k)}, 1\right\} & \text{if} \quad s_i^{(k)} \ge \min\left\{(1+\zeta)\rho_i^{(k)}, 1\right\} \end{cases}, \qquad (2.3)$$

where ζ was the move limit (in this work, values of 0.1 to 0.3 were found to be suitable). The term, s_i, was found by,

$$s_i^{(k)} = \left[\frac{1}{\Lambda^{(k)}} \frac{\partial C\left(\rho^{(k)}\right)}{\partial \rho_i^{(k)}} \right]^{\alpha} \rho_i^{(k)}, \qquad (2.4)$$

where *C* was the compliance of the finite element model. The Lagrange multiplier for the volume constraint, Λ, was controlled by,

$$\Lambda^{(k+1)} = \min\left\{ 0, \left[\frac{1}{m_s} \sum \rho_i^{(k)} \right]^{\alpha} \Lambda^{(k)} \right\}, \qquad (2.5)$$

where m_s was the mass constraint. This was related to the volume constraint by, $m_s = V_c \cdot n_{alements}$, where V_c was the volume constraint and $n_{elements}$ was the number of elements in the model.

The purpose of the volume constraint was to fix the sum of the element densities in the structure and hence control the amount of material present. When it comes to

the practical application of topology optimization, this value is somewhat arbitrary since the analysis is linear and material properties used in the final design can be selected later to give the desired structural performance. Hence, for this class of problem, the topology results only indicate the basic shape of an efficient structure and do not provide an accurate and detailed model of the final design.

2.2 Methodology

2.2.1 Finite Element Models

The FEA models used for the topology optimization consisted of grids of 8-noded brick elements of identical size and shape. This type of modeling was necessary to allow the use of the computationally efficient method described in Section 2.1.2. Since the spoiler has a tapered region at the edge of the design envelope of maximum X value (i.e. the trailing edge), the finite elements were arranged in steps. Figure 2.1 shows a model of the spoiler in a deflected state. There are 3 steps visible in the tapered region and the near end of the model has symmetry in the XY plane.

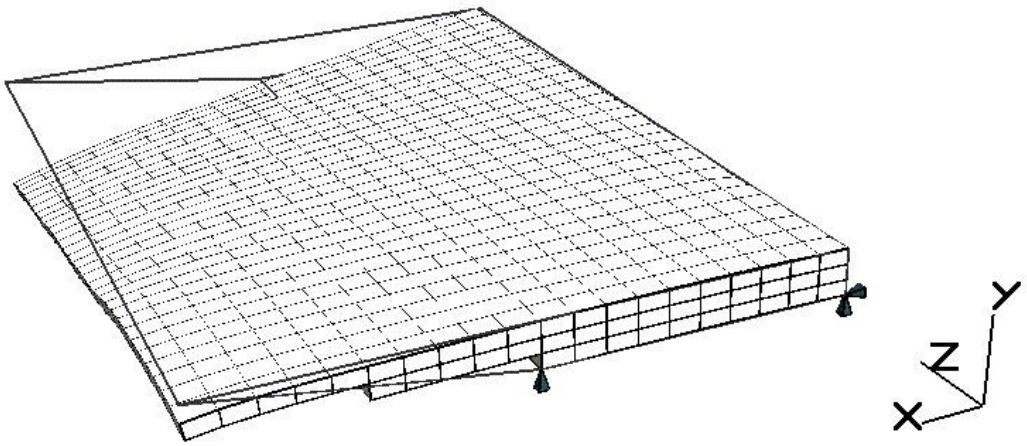

Figure 2.1, A finite element model of the deflected spoiler with three steps of elements in the tapered region.

In general, thin-panel aircraft structures have more complex geometry than the spoiler considered in this study and hence significantly more element steps might be required. The applicability and accuracy of the stepping approximation was investigated during this study and is discussed in the conclusion.

Topology optimization results are only as useful as the nearest manufacturable designs they suggest. If typical thin-skinned, planar structural features (e.g. skins, ribs, spars, stiffeners, etc.) of the topology-optimized results are to be immediately recognizable, the results must consist of planar or near-planar arrangements of high-density elements. However, due to computational limitations, the finite elements in this study were thicker than typical spoiler skin panels. Hence, some inaccuracies resulted during the interpretation of the topologies into thin-panel structures. Clearly, using smaller element dimensions makes the interpretations more accurate.

2.2.2 Visualization of Results

To facilitate visualization of the topology optimization results, a number of steps were taken. Firstly, the boundaries of the design envelope were included as grey lines in the images and small pyramids indicated the locations of the boundary constraints (excluding those enforcing symmetry). Figure 2.1 also shows these features.

To clearly display the interior details of the topology optimization results seen later in this paper, all elements with a density below 0.5 were made invisible. In addition, a color scheme was used to highlight the interior structure; elements on the top surface were shaded in light gray, elements on the lower and side surfaces were shaded in a dark gray and interior elements were shaded in a medium gray. Also, an algorithm[1] to lift away an entire skin of the model (top or bottom) to allow an unrestricted view of the interior was used.

[1] This algorithm is not discussed here, as it is not relevant to the main themes of this research.

2.2.3 The Checkerboard Fill-In Algorithm

One further problem whilst interpreting topology optimization results is the occurrence checkerboard patterns. Diaz & Sigmund (1995) gave a thorough investigation of the checkerboard problem. In Sigmund & Petersson (1998) reported on various methods for avoiding it and similar numerical instabilities in topology optimization. Further, they stated that methods whereby the optimal solution is obtained (with checkerboards) and is then *smoothed* should be avoided since that ignores the underlying problem. However, for simplicity a smoothing approach was taken in this work and the use of this method is justified in the conclusion.

When a checkerboard pattern is present in limited quantities, structural features are often recognizable although the accuracy of the interpreted design's structural performance (e.g. stiffness to weight ratio) can be questionable. In this work, it was proposed to consider partially checkerboarded designs as valid after some filtering or smoothing was performed. The filtering was a post-processing step that filled-in the low-density elements in checkerboarded regions. The amount of material that needed to be filled-in gave estimates of the severity of the initial checkerboard.

The checkerboard fill-in algorithm scanned the densities of all elements, *i*, in the model. If four or more of the six directly neighbouring elements (given by the index *j*) sharing a face with element *i* satisfied the condition,

$$\rho_j > \rho_i + 0.5, \tag{2.6}$$

the density of element *i* was changed by,

$$\rho_i = \max\{\rho_j\}. \tag{2.7}$$

This algorithm corrected for 3D checkerboard in any of the 3 possible planes. Figure 2.2 shows a 2D example of this checkerboard fill-in process. Note that each white element that becomes black does so due to the density of its neighbours.

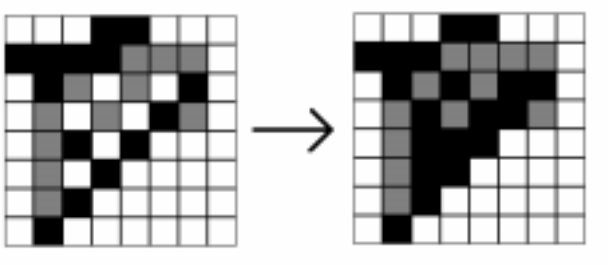

Figure 2.2, 2D example of the checkerboard fill-in algorithm
(white is zero density, gray is low density, dark is high density)

Appendix B contains a review of a number of topology optimization control strategies (both existing and novel) that were considered for this work. As none of the methods were utilized, the appendix is provided merely as a loose collection of information for researchers interested in this issue.

2.3 Investigations

An exploration of the parameters that influence the features of the optimized topologies was made. The following sections present a summary of these investigations. The parameters of interest were the volume constraint and the mesh dimensions. The features of the topologies that were examined were surface coverage, specific stiffness and the ability to recognize internal structural features in the solutions.

2.3.1 Variation of Mesh Dimensions and Volume Constraint

In order to examine the influence of mesh density and volume constraints on the final topologies, experiments were performed with a range of input values. Mesh dimensions were varied over the sets: {20 x 3 x 30}, {26 x 4 x 40}, {30 x 5 x 50}, {36 x 6 x 55} and {40 x 7 x 60}. These sets of dimensions produced models with

1350, 3080, 5550, 8745 and 12360 elements respectively. The highest element aspect ratio[2] from these choices of mesh dimensions was 2.31 for the {40 x 7 x 60} case.

Simultaneously, the volume constraint, V_C, was varied over the values 0.4, 0.5, 0.6, 0.7 and 0.8. Significantly different topologies were given in each case and the topologies resulting from the four extremes of the input parameters are shown in Figures.2.3 a) & b). All the topologies had top skins that closely resembled the bottom skins. Hence, the top skins have been removed from these images to visualize the interior structural features.

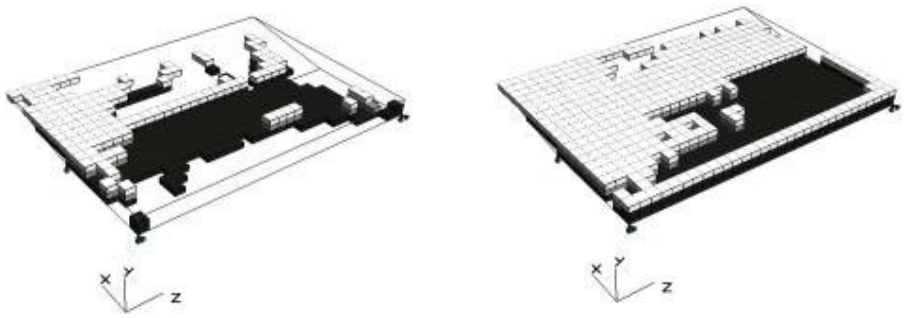

Figure 2.3 a), Optimized models for 20 x 3 x 30 mesh; V_C =0.4 (left), V_C =0.8 (right).

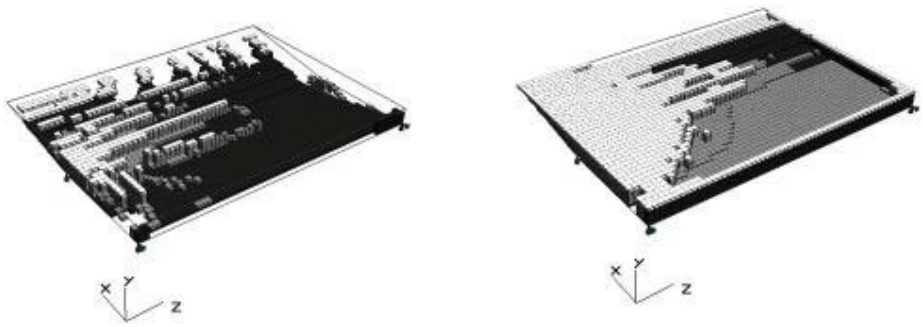

Figure 2.3 b), Optimized models for 40 x 7 x 60 mesh; V_C =0.4 (left), V_C =0.8 (right).

[2] Element aspect ratio is the ratio of maximum side length to minimum side length. Excessive values can produce inaccurate FEA results.

In general, the smaller mesh sizes produced topologies that had significant gaps in the top and bottom skins. Also, lower volume constraints made the interiors relatively empty and high volume constraints tended to fill the interiors. Also, the combination of low volume and low mesh size in the left image of Figure 2.3 a) made both the interior and surface of the topology quite empty. These trends are quantified in the following sections.

2.3.2 Surface Coverage

In this work, surface coverage was defined as the average density of all elements on the exterior of the model, and was expressed as a percentage. Table 2.1 and Figure 2.4 summarize the surface coverage for the optimized topologies resulting from the 25 different combinations of mesh dimensions and volume constraints considered in this study.

No. Elements	Volume Constraint (V_C) 0.4	0.5	0.6	0.7	0.8
1350	52.2	62.1	72.6	86.5	93.2
3080	60.4	71.7	86.4	93.2	97.3
5550	65.7	80.9	90.0	95.6	96.7
8745	72.5	87.1	93.3	94.0	96.9
12360	80.1	88.9	92.8	95.0	97.6

Table 2.1, Surface Coverage for a range of volume constraints and number of elements.

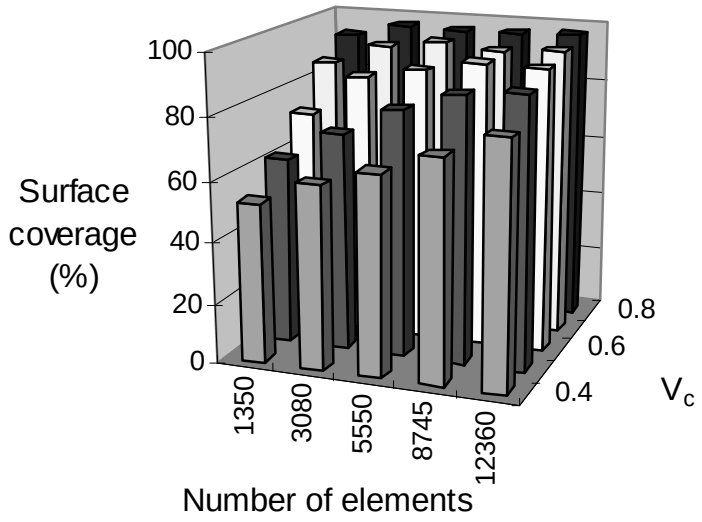

Figure 2.4, Surface Coverage for a range of volume constraints and number of elements.

The surface coverage was seen to be dependant on both the mesh dimensions (indicated by the number of elements) and the volume constraint. The combination of a low volume constraint and low number of elements produced the lowest surface coverage of about 50%. Combinations of optimization parameters with either a high number of elements or high volume constraints produced high surface coverage of about 90%.

2.3.3 Specific Stiffness

Another quantity that can be measured from these results is the specific stiffness. This is equal to 1/Weight/Compliance and hence has the units $(kg.m.N)^{-1}$. In general an efficient structure will have high specific stiffness. For the purpose of the specific stiffness comparison, a density of 540 kg/m^3 and a Young's modulus of 14 GPa were assumed. These values are arbitrary since the analysis and optimization is linear.

No. Elements	Volume Constraint 0.4	0.5	0.6	0.7	0.8
1350	9.19	9.44	9.34	9.06	8.49
3080	9.99	9.97	9.61	8.82	8.01
5550	10.1	10.1	8.85	8.48	7.73
8745	10.4	9.85	8.85	8.12	7.34
12360	10.8	9.85	8.83	8.15	7.31

Table 2.2, Specific stiffness for a range of volume constraints and number of elements (NB. all values must be multiplied by 10^{-3})

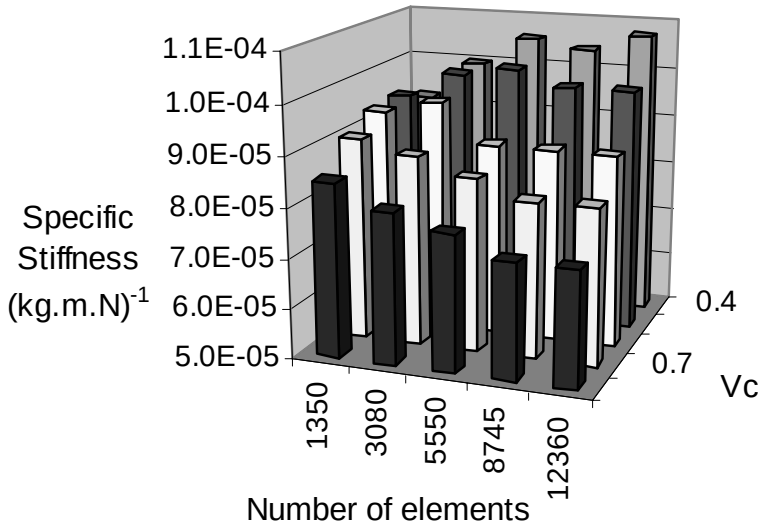

Figure 2.5, Specific stiffness for a range of volume constraints and number of elements.

2.3.4 Recognizable Internal Members

In Figure 2.3 b), the light colored elements are part of the top layer of the mesh and hence indicate the presence of internal structure connecting the top to bottom skins. The left image in Figure 2.3 b) contains elongated spar-like members whereas the topology on the right of Figure 2.3 b) consists only of a block of material clustered around the center.

From the point of view of composite manufacturing, solid core material (foam or honeycomb) is needed to produce such designs. However, in the earlier work forming the basis for this research (Ness *et al.*, 1998), the use of honeycomb or foam filled core structure was undesirable due to moisture uptake concerns. Hence, in this research, designs with *panel-type* interior structure (e.g. spars or ribs) were favored over *core-type* interiors.

An algorithm was used to quantify the relative abundance of *panel-type* and *core-type* interior structure. This algorithm used the density distributions to identify locations in the XZ plane corresponding to 3 distinct types of internal structure; *core-type* structure, *panel-type* internal elongated members (e.g. spars or ribs) and *non-connected* (only top and bottom skins with no internal structure). Columns (in the Y-axis) of high-density elements that were surrounded by other columns were classified as *core-type* while high-density columns that had at least one side with low-density elements were classified as *panel-type* members. All remaining columns had 1 or more low-density elements and hence were classified as *non-connected*, since the upper and lower skins were not connected at that XZ location. The proportions of each type of internal structure present in each topology were expressed as a ratio of the area of the spoilers design volume projected onto the XZ plane. The variables 'A', 'B' and 'C' were used to represent these ratios and correspond to *panel-type* members, *core-type* structure and *non-connected* internal structure respectively.

As such, the ratio A/B (panel-type to core-type) is a good indicator of the ability to recognize useful interior structural features since it favors a high proportion of elongated internal members and a low proportion of internal core structure. For other design tasks where core-type structure is feasible, the A/B ratio would not be relevant.

Figure 2.6 shows a clear maximum value for A/B in the case of a 0.4 volume constraint and with 12360 elements. Hence, the left image in Figure 2.3 b) shows the topology with the most clearly defined internal panel-type members. A trend for A/B to increase with increasing elements is evident. For all cases where the volume constraints were 0.6 or less, the A/B ratio was not far below 1.0. Hence, all these topologies contain at least some recognizable *panel-type* internal structure. In the

cases with the volume constraint above 0.6, the topologies had very low A/B due to the abundance of core-type structure.

No. Elements	Volume Constraint 0.4	0.5	0.6	0.7	0.8
1350	0.94	0.99	0.80	0.41	0.26
3080	1.54	1.44	0.85	0.28	0.16
5550	2.06	1.44	1.05	0.35	0.29
8745	2.25	1.82	0.79	0.56	0.27
12360	8.03	1.45	1.29	0.71	0.22

Table 2.3, A/B ratio for a range of volume constraints and number of elements.

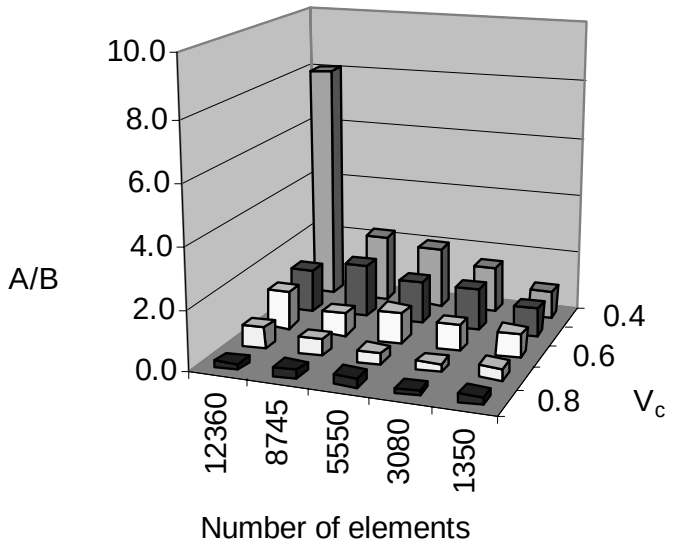

Figure 2.6, Panel to core ratio for a range of volume constraints and number of elements.

2.4 Conclusion

2.4.1 Selection of a Best Design

Although the range of parameters was limited, some clear trends were seen in these investigations. High mesh densities and low volume constraints gave high levels

of A/B whilst also providing acceptable surface coverage. Also, the specific stiffness was best for the same choices of parameters. Hence, the design with 12360 elements and a 0.5 volume constraint was chosen as the best design in a compromise between A/B and surface coverage. Figure 2.7 shows top and bottom views of this design.

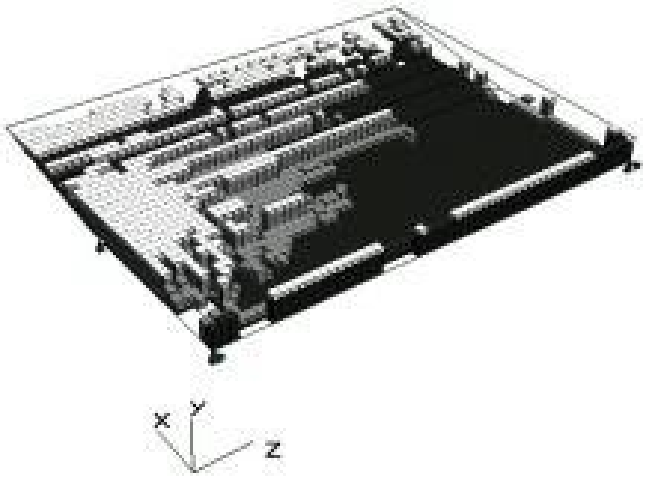

a)

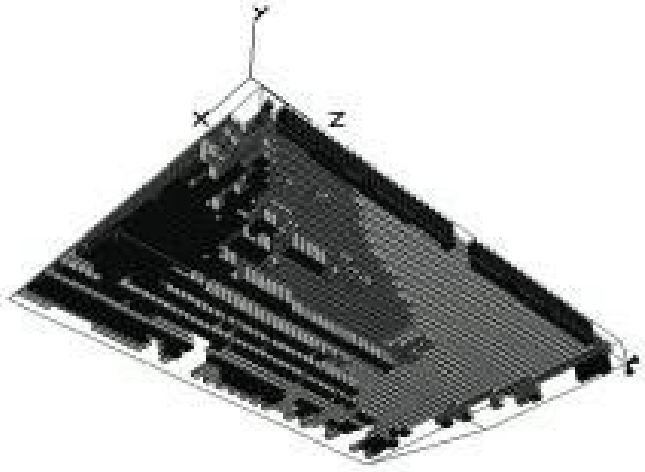

b)

Figure 2.7, Best design; a) Top view with top skin removed,
b) bottom view with bottom skin removed

The presence of some *core-type* structure near the actuator jack is considered acceptable since previous work assumed the use of metallic fittings to distribute the concentrated load at this location. A number of members resembling conventional

spars extend from the actuator position. These ‘semi-span spars’ were not seen in any of the earlier work and hence, may represent a new feature to be considered in future designs. The stress raising effect of including such terminating spars should be considered if they are to be used in real designs.

In the vicinity of the centre hinge are holes in both the top and bottom skins (at the corner nearest the axes symbols in the models in Figure 2.7). Such results indicate that supporting the centre hinge reaction does not require a conventional center rib connected to the actuator jack. Rather, a diagonal member at approximately 45° away from the main spar is more efficient. This feature was also seen in the earlier work by Ness *et al.* (1998).

Towards the tapered trailing edge there are a number of spar-type members that are aligned with the steps of the finite element mesh. This suggests that the steps were biasing the designs in the tapered region. Figure 2.7 b) shows some details of possible ply drop-offs and/or stiffened regions on the underside of the top skin.

This design includes neither a complete main spar nor an end rib. This is possibly due to relatively thicker element dimensions in the X and Z directions. Since the incomplete structure present in these locations clearly transmits some shear loads between top and bottom skins, a design with a completely closed end rib and main spar would be a sensible interpretation of this topology.

Towards the tapered edge, a non-uniform material distribution was seen in most of the designs with volume constraint below 50%. Figure 2.3 b) shows thickened finger-like extensions at somewhat equally spaced intervals along the underside of the trailing edge. This type of topology feature could be realized in a real composite spoiler design by using ply drop-offs in finger shapes. Such a design contrasts with the previous suggestions (Ness *et al.*, 1998) where a full-span, wedge shaped foam insert was suggested to form the trailing edge.

2.4.2 Discussion on the Methodology

This investigation has provided a new perspective on a number of issues relating to the structurally efficient design for the generic spoiler and other thin-skinned stiffened structures. The Density method used in conjunction with the checkerboard fill-in algorithm was able to provide topologies that could be converted into feasible designs. The use of a variety of input parameters was shown to strongly influence the resulting topologies. Hence, the quantitative measures (metrics) of surface coverage, specific stiffness and panel-to-core ratio were useful in comparing the feasibility and efficiency of the various topologies.

The surface coverage metric was an indicator of the practicality of a topology since real spoilers require completely covered skins to properly function as aerodynamic surfaces. A constraint to guarantee the existence of material on the skins could have been used however such a strategy would not have indicated the optimal quantity of interior structure. Specific stiffness was shown to be strongly dependent on the volume constraint and performing optimization runs with a range of volume constraints was beneficial. The A/B ratio introduced in Section 2.3.4 was demonstrated to effectively quantify the proportions of interior *panel-type* structure for this particular design problem where *core-type* structure was undesirable.

The use of 3D topology optimization shed new light on the spoiler design problem. In particular, the optimal location of through the thickness structural features (e.g. spars, ribs, etc.) did not always coincide with that of skin stiffening (e.g. thickened skin areas, stiffeners, etc.). Also, the topology in Figure 2.7 suggested that efficient design for regions of point load input (e.g. hinges, jacks, etc.) can involve complex 3D geometry.

There was a conspicuous absence of a closed torsion box on some of the designs with low volume constraints. In the designs without a closed torsion box, the shear forces acting between top and bottom skins were transmitted purely through the internal structure rather than through the outer panels of a closed torsion box. Whilst Section 2.3 showed that topologies of this type are less efficient from a purely structural perspective, they are also considered sub-optimal under real world

conditions since closed torsion boxes are more durable during manufacturing and off-design load cases.

The checkerboard fill-in algorithm was demonstrated to produce recognizable features in the optimized topologies of this research. Hence, the use of this method is justified in the context of this work. However, it is likely that one of the more advanced checkerboard elimination schemes discussed by Sigmund & Petersson (1998) would have produced different results. The majority of existing work on checkerboard problems focussed on 2D problems. Hence, the fact that this work involved entirely 3D models may be a reason for the relative success of the simplistic checkerboard removal approach that was taken.

This work has shown that a limited quantity of interior structure is efficient from the point of view of linear static structural efficiency. Designing for non-linear skin deformations such as buckling and large displacements would probably require more internal complexity (stiffened skins, etc.) but is difficult to model in sparse PCG-based topology optimizations of this type. Similarly, local stress raising effects due to terminating internal members and other features require different design tools to be treated effectively. As such, the topology optimization methodology presented here is only a preliminary design aid for determining the fundamental features of efficient thin-panel structures.

References

Diaz, A.R., Sigmund, O., 'Checkerboard Patterns in Layout Optimization', *Structural Optimization*, 10, 1, 40-45, 1995.

Fujii, D., Suzuki, K., Ohtsubo, H., "Topology Optimization of Structures using the Voxel Finite Element Method", *Trans, JSCES, paper no. 2000, in Japanese,* 2000.

García, M. J., Steven, G. P., "Interactive aerospace design using fixed grid finite element analysis", *International Aerospace Congress, Sydney,* 1997.

Hollister, S. J., Kikuchi, N., “Homogenization theory and digital imaging: a basis for studying the mechanics and design principals of bone tissue”, *Biotechnology and Bioengineering*, 43, No. 7, pp. 586-596, 1994.

Ness, R., Wang, J., Kelly, D., Raju, J., Barton, A., Lindsay, A., “Conceptual Design of a Wing Spoiler”, *Technical Report CRC-ACS CP 98011, Cooperative Research Centre for Advanced Composite Structures, Australia,* 1998.

Sigmund, O., Petersson, J., “Numerical Instabilities in Topology Optimization: A survey on Procedures Dealing with Checkerboards, Mesh-Dependencies and Local Minima”, *Structural Optimization*, **16**, 68-75, 1998.

Suzuki, K., Kikuchi, N., “A homogenization Method for Shape and Topology Optimization”, *Comp. Meth. In App. Mech. and Eng.*, **93**, 291-318, 1991.

Suzuki, K., Ohtsubo, H., Terada, K., "The analysis method of 3D solid using multi-voxel data", *Proceedings IACM WCCM IV, Buenos Aires*, 1997.

Van Der Vorst, H., Dekker, K., “Conjugate Gradient Type Methods and Preconditioning”, Journal of Comp. and Appl. Math., **24**, 73-87, 1988.

Yang, R. J., Chuang, C. H., “Optimal Topology Design Using Linear Programming”, *Computers & Structures*, Vol. 52, No. 2, pp. 265-275, 1994.

Zhou, M., Rozvany, G. I. N., “The COC Algorithm, Part II: Topological, Geometrical a Generalized Shape Optimization”, *Comp. Meth. in App. Mech. and Eng.*, 89, 309-336, 1991.